Optics Letters

Sub-second hyper-spectral low-frequency vibrational imaging via impulsive Raman excitation

Dekel Raanan,[1,†] Xavier Audier,[2,†] Siddarth Shivkumar,[2,†] Maor Asher,[3] Matan Menahem,[3] Omer Yaffe,[3] Nicolas Forget,[4] Hervé Rigneault,[2,*] and Dan Oron[1]

[1]Department of Physics of Complex Systems, The Weizmann Institute of Science, Rehovot 76100, Israel
[2]Aix Marseille Univ, CNRS, Centrale Marseille, Institut Fresnel, Marseille, France
[3]Department of Materials and Interfaces, The Weizmann Institute of Science, Rehovot 76100, Israel
[4]Fastlite, 06600 Antibes, France
*Corresponding author: herve.rigneault@fresnel.fr

Received 4 June 2019; revised 5 September 2019; accepted 20 September 2019; posted 23 September 2019 (Doc. ID 368972); published 17 October 2019

Real-time vibrational microscopy has been recently demonstrated by various techniques, most of them utilizing the well-known schemes of coherent anti-stokes Raman scattering and stimulated Raman scattering. These techniques readily provide valuable chemical information mostly in the higher vibrational frequency regime (>400 cm^{-1}). Addressing the low vibrational frequency regime (<200 cm^{-1}) is challenging due to the usage of spectral filters that are required to isolate the signal from the Rayleigh scattered excitation field. In this Letter, we report on rapid, high-resolution, low-frequency (<130 cm^{-1}) vibrational microscopy using impulsive coherent Raman excitation. By combining impulsive excitation with a fast acousto-optic delay line, we detect the Raman-induced optical Kerr lensing and spectral shift effects with a 25 µs pixel dwell time to produce shot-noise limited, low-frequency hyper-spectral images of various samples.

https://doi.org/10.1364/OL.44.005153

The Raman effect, which describes the inelastic scattering of light due to the induced-dipole interaction between light and molecules, has become a leading tool in performing vibrational spectroscopy and label-free chemically selective optical microscopy. While chronologically the spontaneous process was first discovered and used, further development of laser sources (especially of mode-locked lasers) enabled the usage of coherent, stimulated Raman scattering (SRS) techniques [1–3]. Those processes both stimulate the vibration coherently throughout the sample and further detect it, producing significantly stronger signals compared to the diffuse spontaneous process, thus allowing for vibrational imaging of biological samples on a short timescale [4–11].

The molecular vibrational spectrum spans from high frequencies around 3300 cm^{-1}, which are usually associated with C-H and O-H stretch modes, continues in the fingerprint region between 400 cm^{-1} and 1400 cm^{-1}, and ends at the low-frequency vibrations at wavenumbers below 200 cm^{-1}. While the 200–3300 cm^{-1} range includes mostly localized intramolecular vibrations and, hence, provides information about the building blocks of the sample, the low-frequency region is typically associated with a collective motion of multiple atomic and molecular groups, providing information about the overall molecular organization [12–17]. Vibrational spectroscopy is ordinarily done in the higher frequency range, by either coherent anti-Stokes Raman scattering (CARS) or SRS, typically pumped by two narrowband laser sources whose energy difference is tuned to the vibrational resonance. However, performing low-frequency vibrational spectroscopy and microscopy was found to be challenging and, therefore, experimental work in this frequency range has been relatively sparse. The reason for this difficulty is that both CARS and SRS rely on optical chromatic filters that are used to isolate the Raman signal from the input fields. Since typical high-quality optical edge filters available on the market today have a 40–60 cm^{-1} transition slope, lower frequencies can only be detected by considerably increasing the integration time, which prevents fast imaging.

Time-resolved coherent impulsive techniques, which detect the transient response of a molecular vibration, have found great promise in performing single-beam Raman spectroscopy and microscopy [18–21]. These techniques rely on high temporal resolution of the excitation pulse rather than on high spectral resolution which is used by the more conventional CARS and SRS techniques [12,18,19]. Hence, by observing the temporal dynamics that follow an excitation of the sample, the low-frequency challenge translates from the ability to spectrally scan and separate fields with nearby wavelengths to scanning delays between the excitation and probe pulses. The roots for such time-domain techniques can be found in the early 1990s [12,18]; however, the laser source used was an amplified

ultrafast oscillator with a relatively low repetition rate and high energy per pulse, which impedes its usage in biological microscopy applications.

In this Letter, we demonstrate sub-second (25 μs pixel dwell time) low-frequency hyper-spectral (20–130 cm^{-1}) vibrational spectroscopy and microscopy of various samples by combining an impulsive time-domain detection apparatus and a fast acousto-optic programmable dispersive filter (AOPDF) delay line. Our shot-noise limited detection system identifies fine modulation transfer between a modulated pump pulse and an unmodulated probe pulse.

Raman-induced Kerr lensing [22,23] and Raman-induced spectral shifts [12,18,24–26] have recently been demonstrated with low-energy pulses. Both can be described by an oscillating refractive index that is induced by a pump pulse that affects a delayed probe pulse. The Raman-induced Kerr lensing effect is similar to the third-order electronic Kerr effect; however, it is non-instantaneous, as the molecular vibration persists past the duration of the excitation pulse, which results in alteration of the refractive index at nonzero delays. The spatial profile of the pump beam imprints a similar distribution on the vibration amplitude of the molecules in the sample and, as a consequence, molecules that are placed at the center of the beam are more strongly driven compared to the molecules that are placed at the margins of the beam. Since the refractive index is altered by the molecular vibration, it results in a lens-like effect. Therefore, the variation of the refractive index with time associated with the molecular vibration can be probed via a change of the spatial extent of a delayed (probe) pulse in the far-field. The same time-variant refractive index also affects the spectral profile of the pulse via phase modulation. The time derivative of the oscillating refractive index results in a phase modulation and a corresponding spectral shift of the probe's spectrum which depends on the phase of the vibration as the probe passes through the sample. After the time response of the sample has been detected, a Fourier transform of the acquired signal (at positive delays exceeding the pulses durations) reveals the vibrational frequencies.

In order to achieve fast imaging, we scan the delay between the two pulses with an AOPDF (Dazzler, Fastlite), which is a device that creates an acoustic pulse that propagates collinearly with the laser beam through a birefringent crystal [27]. This acoustic wave leads to a rotation of the polarization of the incoming ultrashort pulse by 90 deg, thus changing the polarization of the pulse in the crystal, which results in a change of the effective optical path through the device. Each of the optical pulses that emerge from the laser oscillator encounters the acoustic pulse at a different position along the crystal and, thus, experiences a different delay compared to an optical pulse that travels outside the device [28].

The essence of the experimental setup is similar to the scheme used in our previous works [29,30] and is based on a low-noise pump-probe measurement apparatus with a controlled delay (see Fig. 1). An 800 nm ultrafast oscillator (Chameleon, Coherent) acts as the probe pulse and is frequency converted using an optical parametric oscillator (APE, fs OPO) to produce a pump pulse at 1045 nm. The pump pulse is compressed to 160 fs at the sample plane using a grating compressor, and the probe is compressed to the same duration using the Dazzler itself, which corresponds to an excitation and detection bandwidth of 130 cm^{-1}. We use an acousto-optic modulator

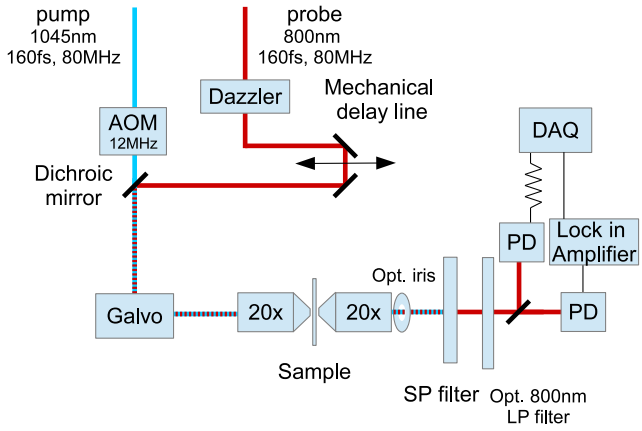

Fig. 1. Experimental setup. AOM, acousto-optic modulator; PD, photodiode; DAQ, data acquisition card.

(MT200-A0.2-1064, AA optoelectronics) at 12 MHz to modulate the pump beam for lock-in detection. The probe passes through the Dazzler and a mechanical delay line. Note that the mechanical delay line is used to adjust the scanning delay range, whereas the Dazzler is used to perform the fast probe pulse delay scan. The beams are recombined by a dichroic mirror and are scanned onto the sample by a galvanometric mirror pair. The beams are focused and collected in the forward direction from the sample by a pair of identical 20× 0.75 NA objectives (0.75 NA, CFI Plan Apo Lambda, Nikon). Afterwards the beams are spectrally filtered to block the pump beam (FES0900, Thorlabs). The probe is detected with two large-aperture photodiodes, one for the detection of the modulation transfer from the pump to the probe (SRS lock-in module, APE) and the other for the detection of the integrated transmission of the probe (DET100A, Thorlabs). The demodulated output from the lock-in amplifier was electronically low-pass filtered to 1.35 MHz (EF508 Thorlabs, 5th order). The signal from the lock-in was sent to a data acquisition card (ATS460, AlazarTech) and acquired with a sampling rate of 10 MHz. In order to detect Raman-induced Kerr-lensing, a clipping iris, placed at the back focal plane of the collection objective, translates the change of the extent of the beam due to the Raman interaction to a change of intensity. For the measurement of Raman-induced spectral shift, a long-pass filter at 800 nm (FELH0800, Thorlabs) splits the probe spectrally around the center of the spectrum and translates the spectral shift into an intensity variation onto the detector. The average powers of the pump and probe beams at the sample were adjusted to 33 and 37 mW, respectively. The plotted signal in the following figures is the modulated component from the lock-in amplifier normalized by the spatial integration of the DC channel over the full image (which compensates for the slight delay dependence of the transmission of the Dazzler). In all measurements, we used an integration time of 300 ns per delay point with the APE lock-in amplifier. A single hyper-spectral acquisition for one pixel requires 25 μs, which is the time it takes the acoustic wave to travel through the Dazzler. During this period, the data acquisition card accumulates 264 data points.

The AOPDF delay line used (Dazzler WB) is capable of providing delays up to 3.5 ps. In order to fully characterize

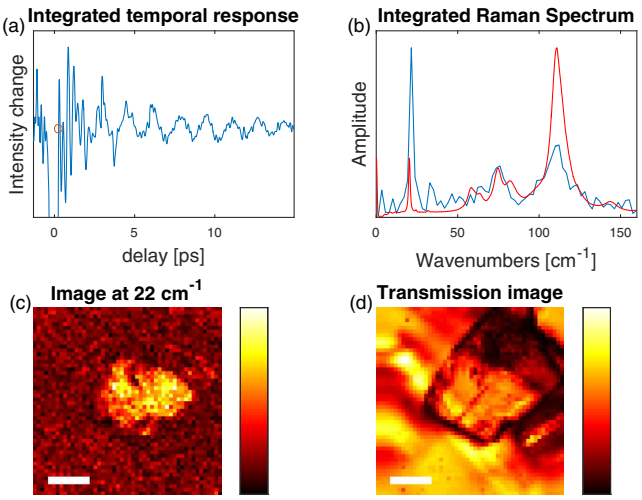

Fig. 2. CBZ DH crystal as measured with the Raman-induced Kerr lensing technique. (a) Image-integrated oscillations of the measured modulated intensity as a function of the pump-probe delay. (b) Fourier transform of the time-domain oscillations resolves the vibrational frequencies of the molecules (blue) that can be compared with the spontaneous Raman spectrum from the same sample (red). The Fourier analysis begins at the red circle in (a). (c) Image resolved around 22 cm^{-1} shows features on the crystal. (d) Transmission image of the crystal. Scale bar: 20 μm.

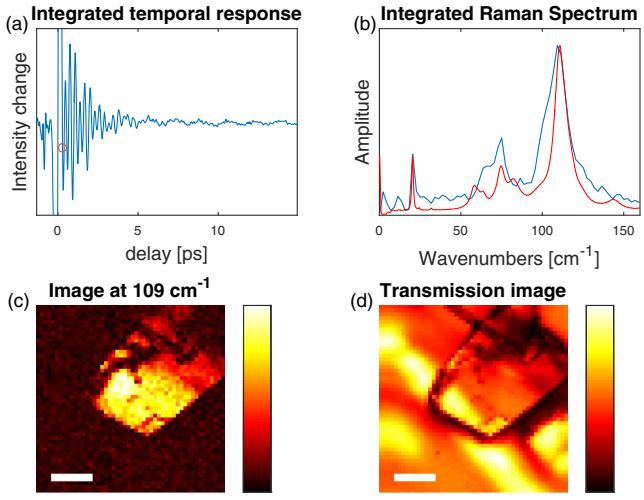

Fig. 3. CBZ DH crystal as measured with the Raman-induced spectral shift technique. (a) Image-integrated oscillations of the measured modulated intensity as a function of the pump-probe delay. (b) Fourier transform of the time-domain oscillations resolves the vibrational frequencies of the molecules (blue) that can be compared with the spontaneous Raman spectrum from the same sample (red). The Fourier analysis begins at the red circle in (a). (c) Image resolved around 109 cm^{-1} shows the features of the crystal. (d) Transmission image of the crystal. Scale bar: 20 μm.

the molecular ringing that follows an excitation and possibly extend the Dazzler delay range (leading to an enhanced spectral resolution), we translated the mechanical delay line and stitched the data from the separated span measurements.

As a demonstration, we show the molecular ringing and the extracted Raman spectrum of a carbamazepine dihydrate (CBZ DH) crystal in Figs. 2(a) and 2(b), respectively, using the Raman-induced Kerr lensing technique (blue curves). We note that we begin the Fourier analysis of Fig. 2(b) only at times at which the probe pulse no longer overlaps the pump pulse, as marked by a red circle at 260 fs in Fig. 2(a). Commercial CBZ powder was purchased from Sigma Aldrich Chimie S.a.r.l (St. Quentin Fallavier, France). CBZ DH was prepared by recrystallization from an ethanol-water mixture (50/50) via slow evaporation at room temperature [31]. For comparison, the spontaneous Raman spectrum, obtained with a custom built backscattering Raman spectrometer based on a Horiba FHR-1000 dispersive spectrometer, is shown in Fig. 2(b) in red. Notably, the spectral resolution is determined by the maximal measured delay which, in turn, is determined by the signal-to-noise ratio of our measurements. In Fig. 2(c), we show the image of the CBZ DH crystal as measured at 22 cm^{-1} over a field of view of 100 μm × 100 μm and, in Fig. 2(d), we show the transmission image from the sample acquired at the same time. To obtain this time trace, Raman spectrum, and image, we stitched data of five different delays with the mechanical delay line, which results in a total integration time of 0.375 s.

Figure 3 shows an image of the same CBZ DH crystal as measured with the spectral shift technique (blue curves in a and b). As before, we begin the Fourier analysis that is shown in Fig. 3(b) at the red circle that appears at 290 fs in Fig. 3(a). A vibrational spectrum similar to the one shown in Fig. 2(b) is detected; however, we note the different ratio between the vibrational bands. The reason for this is that the Raman-induced Kerr technique is related to the refractive index, as opposed to the spectral shift technique (and to spontaneous Raman scattering) which is related to the time derivative of the refractive index, leading to phase modulation. This makes the Raman-induced Kerr technique more sensitive to slow vibrations.

Figure 3(c) shows the acquired image corresponding to the 109 cm^{-1} line, and Fig. 3(d) shows the transmission image through the crystal. Here we also stitched data from five different delays, which resulted in a total integration time of 0.375 s.

We also show the molecular ringing and the extracted Raman spectrum of an anthracene crystal in Figs. 4(a) and 4(b), respectively, using the Raman-induced Kerr lensing technique (blue curves). We begin the Fourier analysis of Fig. 4(b) at the point that is marked by a red circle at 400 fs in Fig. 4(a). The spontaneous Raman spectrum is shown in Fig. 4(b) in red. As before, the main reasons for the difference in the ratio between different lines in our measurement as compared to the spontaneous Raman measurement are the technique itself which enhances low frequencies over higher frequencies and the limited bandwidth of our pulses. In Fig. 4(c), we show the image of the anthracene crystal at 37 cm^{-1} over a field of view of 200 μm × 200 μm and, in Fig. 4(d), we show the transmission image from the sample acquired at the same time. Since the signal from anthracene is weaker than the signal from CBZ DH, an average was performed over 10 images. To obtain this time trace, Raman spectrum, and image, we stitched data of four different delays with the mechanical delay line, which results in a total integration time of 3 s. We note that for this measurement we modulated the acousto-optic modulator at 20 MHz.

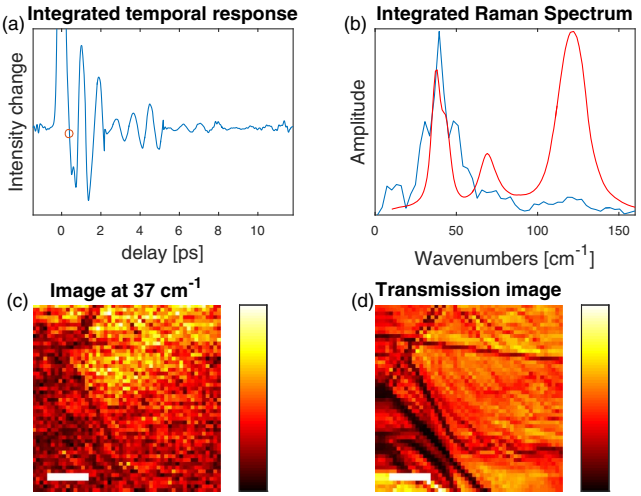

Fig. 4. Anthracene crystal as measured with the Raman-induced Kerr lensing technique. (a) Image-integrated oscillations of the measured modulated intensity as a function of the pump-probe delay. (b) Fourier transform of the time-domain oscillations resolves the vibrational frequencies of the molecules (blue) that can be compared with the spontaneous Raman spectrum from the same sample (red). The Fourier analysis begins at the red circle in (a). (c) Image resolved around 37 cm^{-1} shows features on the crystal. (d) Transmission image of the crystal. Scale bar: 40 μm.

In Ref. [30], we showed that our low Raman imaging system (laser and detection electronics) is shot-noise limited, therefore providing the ideal platform to perform low Raman fast hyperspectral imaging. One of the advantages of time-domain measurements over spectral domain measurements is the sensitivity to the vibrational phase, thus providing additional information as compared to frequency-domain Raman measurements. We found that the Dazzler provides a convenient platform for scanning a relatively large delay range, in line with the beam path, with an unprecedented rate. However, this limits the integration time from above, as required with relatively weak signals. Therefore, the only option for increasing the signal-to-noise ratio is by averaging multiple measurements. While the Raman-induced Kerr effect has an advantage over the spectral shift technique at low vibrational frequencies, it should be noted that it is less straightforward to align experimentally, as one should optimize both the aperture size and its position.

In conclusion, we have demonstrated low-frequency hyperspectral Raman imaging using a shot-noise limited detection apparatus and a fast acousto-optic delay line enabling a minimal integration time of 25 μs per pixel, thus serving as a proof of principle for sub-second, hyper-spectral, low-frequency, vibrational-selective microscopy. We demonstrated our low Raman imaging platform on CBZ DH and anthracene crystals that were imaged at Raman lines below 50 cm^{-1} over a field of view of 100–200 μm in sub-seconds to a few seconds. We believe this approach has the potential to be used in low-frequency vibrational bio-imaging applications with relevance to probe the collective vibrational modes of large-scale molecular assemblies.

Funding. Centre National de la Recherche Scientifique (A-M-AAP-ID-17-13-170228- 15.22-RIGNEAULT, ANR-11-IDEX-0001-02); ANR grants France Bio Imaging (ANR- 10-INSB-04-01); France Life Imaging (ANR-11-INSB-0006); Plan cancer INSERM (18CP128-00, PC201508); Israeli Centers for Research Excellence; Israeli Ministry of Science Tashtiot Program (712845); CNRS-Weizmann ImagiNano European Associated Laboratory.

Acknowledgment. The authors would like to thank Yahel Soffer for the sample preparation.

Disclaimer. Nicolas Forget has financial interest in FASTLITE.

†These authors contributed equally to this Letter.

REFERENCES

1. N. Bloembergen, Am. J. Phys. **35**, 989 (1967).
2. R. Begley, A. Harvey, and R. L. Byer, Appl. Phys. Lett. **25**, 387 (1974).
3. H. Rigneault and P. Berto, APL Photonics **3**, 091101 (2018).
4. A. Zumbusch, G. R. Holtom, and X. S. Xie, Phys. Rev. Lett. **82**, 4142 (1999).
5. J.-X. Cheng and X. S. Xie, J. Phys. Chem. B **108**, 827 (2004).
6. E. Ploetz, S. Laimgruber, S. Berner, W. Zinth, and P. Gilch, Appl. Phys. B **87**, 389 (2007).
7. C. L. Evans and X. S. Xie, Annu. Rev. Anal. Chem. **1**, 883 (2008).
8. C. W. Freudiger, W. Min, B. G. Saar, S. Lu, G. R. Holtom, C. He, J. C. Tsai, J. X. Kang, and X. S. Xie, Science **322**, 1857 (2008).
9. P. Nandakumar, A. Kovalev, and A. Volkmer, New J. Phys. **11**, 033026 (2009).
10. D. Fu, G. Holtom, C. Freudiger, X. Zhang, and X. S. Xie, J. Phys. Chem. B **117**, 4634 (2013).
11. C.-S. Liao, M. N. Slipchenko, P. Wang, J. Li, S.-Y. Lee, R. A. Oglesbee, and J.-X. Cheng, Light Sci. Appl. **4**, e265 (2015).
12. S. Ruhman, A. Joly, B. Kohler, L. Williams, and K. Nelson, Revue de physique appliquée **22**, 1717 (1987).
13. G. Walrafen, M. Fisher, M. Hokmabadi, and W.-H. Yang, J. Chem. Phys. **85**, 6970 (1986).
14. M. Walther, P. Plochocka, B. Fischer, H. Helm, and P. Uhd Jepsen, Biopolymers **67**, 310 (2002).
15. B. Fischer, M. Walther, and P. U. Jepsen, Phys. Med. Biol. **47**, 3807 (2002).
16. T. Globus, D. Woolard, T. Khromova, T. Crowe, M. Bykhovskaia, B. Gelmont, J. Hesler, and A. Samuels, J. Biol. Phys. **29**, 89 (2003).
17. K. Brown, S. Erfurth, E. Small, and W. Peticolas, Proc. Natl. Acad. Sci. USA **69**, 1467 (1972).
18. A. Weiner, D. Leaird, G. P. Wiederrecht, and K. A. Nelson, Science **247**, 1317 (1990).
19. Y. Silberberg, Ann. Rev. Phys. Chem. **60**, 277 (2009).
20. N. Dudovich, D. Oron, and Y. Silberberg, Nature **418**, 512 (2002).
21. L. Ren, I. Hurwitz, D. Raanan, P. Oulevey, D. Oron, and Y. Silberberg, Optica **6**, 52 (2019).
22. D. Heiman, R. Hellwarth, M. Levenson, and G. Martin, Phys. Rev. Lett. **36**, 189 (1976).
23. D. Raanan, J. Lüttig, Y. Silberberg, and D. Oron, APL Photonics **3**, 092501 (2018).
24. H. Frostig, O. Katz, A. Natan, and Y. Silberberg, Opt. Lett. **36**, 1248 (2011).
25. S. Domingue, D. Winters, and R. Bartels, Opt. Lett. **39**, 4124 (2014).
26. D. Raanan, L. Ren, D. Oron, and Y. Silberberg, Opt. Lett. **43**, 470 (2018).
27. F. Verluise, V. Laude, J.-P. Huignard, P. Tournois, and A. Migus, J. Opt. Soc. Am. B **17**, 138 (2000).
28. O. Schubert, M. Eisele, V. Crozatier, N. Forget, D. Kaplan, and R. Huber, Opt. Lett. **38**, 2907 (2013).
29. X. Audier, N. Balla, and H. Rigneault, Opt. Lett. **42**, 294 (2017).
30. X. Audier, N. Forget, and H. Rigneault, "Shot noise limited high speed stimulated Raman microscopy," arXiv:1905.11953 (2019).
31. M. Inoue, H. Hisada, T. Koide, J. Carriere, R. Heyler, and T. Fukami, Org. Process Res. Dev. **21**, 262 (2017).